

# AN ANALYSIS OF THE LARGE SCALE $N$ -BODY SIMULATION USING THE MINKOWSKI FUNCTIONALS

TAKAMICHI NAKAGAMI, TAKAHIKO MATSUBARA

Department of Physics and Astrophysics, Nagoya University, Chikusa, Nagoya 464-8603

JENS SCHMALZING

Ludwig-Maximilians-Universität, Theresienstraße 39, 80333 München, Germany

AND

YIPENG JING

Shanghai Astronomical Observatory, the Partner Group of Max-Planck-Institut für Astrophysik, Nandan Road 80, Shanghai 200030, China

*Draft version October 31, 2018*

## ABSTRACT

We analyze the Minkowski functionals with a large  $N$ -body simulation of a standard  $\Lambda$ CDM model, focusing on transition scales between linear and non-linear gravitational evolution. We numerically calculate the Minkowski functionals with sufficient accuracies to investigate the transition scales,  $10$ – $50 h^{-1}$ Mpc. The results are compared with analytic formulae of linear and second-order perturbation theories. We first show that the skewness parameters of the density fluctuations, which are important in second-order analytic formulae of the Minkowski functionals, are in good agreement with the perturbation theory. Considering relative differences between the Minkowski functionals of the analytic formulae and that of the simulation data, we evaluate accuracy levels of the predictions of the perturbation theory. When the straightforward threshold  $\nu$  by density value is used in Minkowski functionals, the accuracy of the second-order perturbation theory is within 10% for smoothing length  $R > 15 h^{-1}$ Mpc, and within a several % for  $R > 20 h^{-1}$ Mpc. The accuracies of the linear theory are 2–5 times worse than that. When the rescaled threshold by volume fraction,  $\nu_f$  is used, accuracies of both linear and second-order theories are within a few % on all scales of  $10 h^{-1}$ Mpc  $< R < 50 h^{-1}$ Mpc.

*Subject headings:* cosmology: theory — large-scale structure of universe — methods: statistical

## 1. INTRODUCTION

The morphological patterns of the large-scale structure in the universe are the consequence of the dynamical evolution of the universe, and thus provide important information on cosmology. The pattern of the clustering of galaxies is described in many ways. For example, Soneira & Peebles (1978) indicated the picture of the hierarchical clustering, and Jeeveer & Einasto (1986) indicated that of the cell structure. Gott, Melott, & Dickinson (1986) (hereafter GMD) proposed a new picture, which is depicted by sponge-like topology of the universe. To capture the topology of the universe, it is useful to look at the three dimensional views of galaxy distributions (Einasto & Miller 1983). The clustering pattern is so complicated that it is difficult to fully describe the pattern by either the hierarchical picture or the cell picture alone.

GMD showed that the large-scale structure of the universe has sponge-like topology by analyzing the CfA1 catalog of galaxies. They examined various cosmological models of the galaxy distribution and quantified the topology by the genus statistic. The CfA1 catalog which GMD used is the redshift survey of about 1,800 galaxies, which is relatively small catalog with respect to the today's standard. After that survey, numerous redshift surveys such as the Las Campanas Redshift Survey (LCRS), the IRAS Point Source Catalog Redshift Survey (PSCz), etc. have been carried out. Recently, the 2-degree Field Galaxy Redshift Survey (2dFGRS) was completed. The Sloan Digital Sky Survey (SDSS) is now in progress. In the SDSS, redshifts of about  $8 \times 10^5$  galaxies are being observed. These surveys are large enough to quantitatively discuss the topology of the large-scale structure on large scales. Topological analysis is one of the major methods to analyze these redshift surveys (see, e.g., Vogeley et al. 1994; Colley 1997; Canavezes et al. 1998; Colley et al. 2000).

The Minkowski Functionals (MFs) are also used as descriptors of the morphology of the large-scale structure. While they are originally mathematical quantities, Mecke, Buchert, & Wagner (1994) applied the MFs to the analysis of the galaxy clustering. Schmalzing & Buchert (1997) provided a computational algorithm to calculate the MFs. The genus statistic is one of the MFs in a certain condition.

The MFs possess complementary information to the two-point correlation function or the power spectrum, which are the most fundamental tools to quantify the clustering pattern. One of the important applications of the genus statistic and the MFs is a Gaussianity test of the primordial density field, which can not be performed by the two-point correlation function or the power spectrum. Any Gaussian field has a universal form of the genus statistic and the MFs as functions of the density threshold. As a result, any deviation from that form indicates the non-Gaussianity of a density field.

Hikage et al. (2003a) analyzed the early SDSS sample using the MFs. They found the MFs of the SDSS are consistent with that of the  $\Lambda$ CDM model. However, their analysis is limited by the cosmic variance because of the smallness of the data, and

the discrimination of models with various parameters is still difficult. Complete SDSS data would distinguish different models in more detail.

When we compare observations with theories, the  $N$ -body simulation plays an important role. A cosmological  $N$ -body simulation was first carried out by Miyoshi & Kihara (1975). Since then, the number of particles in  $N$ -body simulations has been growing every year. Nowadays simulations with the number of particles of over  $10^9$  and the physical size of  $1 h^{-1} \text{Gpc}^3$  have come to be available. Springel et al. (1998) compared the genus calculated from an  $N$ -body simulation, which contains  $256^3$  particles in a  $(240h^{-1} \text{Mpc})^3$  box, with the data of the IRAS 1.2-Jy redshift survey. Hikage et al. (2002) used an  $N$ -body simulation of the  $\Lambda$ CDM model carried out by Jing & Suto (1998), which contained  $256^3$  particles in a  $(300h^{-1} \text{Mpc})^3$  box. They found that the genus statistic of their  $N$ -body simulations is consistent with the one calculated from the data of the SDSS Early Data Release. Recently, Hikage, Taruya, & Suto (2003b) used the Hubble volume simulation with a box size of  $(3000h^{-1} \text{Mpc})^3$  and a number of particles  $N = 10^9$ , and investigate the genus statistics with respect to the biasing effects.

A drawback of using the  $N$ -body simulation in comparing theories and observations is that the  $N$ -body simulation is computationally costly to obtain theoretical predictions of given cosmological models. Fortunately, there are analytic approximations for MFs. The MFs of a random Gaussian field is well-known (Tomita 1986). However, the density field in the universe is not exactly random Gaussian even if the primordial density field is Gaussian, because of the nonlinear evolution effects. Matsubara (2003) derived the analytic approximations of the MFs of weakly non-Gaussian fields, and obtained analytic formulae of the MFs with effects of the weakly nonlinear evolution by applying the second-order perturbation theory. Since in the last formulae is assumed an approximation that the non-Gaussianity is weak, there is a regime that the formulae can be applied. Identifying such regime is indispensable to use the analytic formulae in analyses of the observations, instead of performing computationally costly simulations model by model.

In this paper, we analyze a large  $N$ -body simulation of the large-scale structure using the MFs and investigate the transition scales between linear and non-linear evolution, and compare them with the theoretical formulae. The accuracy levels of the above analytic formulae are identified. We use an  $N$ -body simulation of  $512^3$  particles in a box of  $(1024h^{-1} \text{Mpc})^3$ .

This paper is organized as follows. In §2, we briefly review the concept of MFs and their theoretical formulae. In §3, we explain the computational methods of the MFs. In §4, we analyze the MFs of the simulation data and compare them with the analytic formulae. In this section the comparison of the skewness parameters, which play an important role in weakly nonlinear formulae, is also presented. In §5, we summarize the results and discuss future outlook.

## 2. THE MINKOWSKI FUNCTIONALS

### 2.1. Definitions

Mecke, Buchert, & Wagner (1994) and Schmalzing, & Buchert (1997) proposed the MFs as the geometrical descriptors of the distribution of galaxies. These quantities are originally derived by Minkowski (1903). To define the MFs of galaxy distributions, we first consider isodensity contours of the density contrast  $\delta = (\rho - \bar{\rho})/\bar{\rho}$ , where  $\rho$  is the density field and  $\bar{\rho}$  is the mean density. Then we identify the set of regions  $M$  where the density contrast  $\delta$  exceeds some threshold. We use the threshold  $\nu$  which is defined by  $\nu \equiv \delta_{\text{th}}/\sigma_0$  for the moment, where  $\delta_{\text{th}}$  is the threshold density contrast and  $\sigma_0 \equiv \sqrt{\langle \delta^2 \rangle}$  is the *rms* of the density contrast. There are  $d+1$  MFs in a  $d$ -dimensional space. The case  $d=3$  is of our primary interest. In this case, the MFs correspond to the following quantities: (1) the fractional volume enclosed by contours

$$V_0 = \frac{1}{V} \int_M dV, \quad (1)$$

where  $V$  is the total volume, (2) the surface area per volume

$$V_1 = \frac{1}{6V} \int_{\partial M} d^2A, \quad (2)$$

where the region of the integral  $\partial M$  is the surfaces of the contours, (3) the integrated mean curvature

$$V_2 = \frac{1}{6\pi V} \int_{\partial M} \left( \frac{1}{R_1} + \frac{1}{R_2} \right) d^2A, \quad (3)$$

where  $1/R_1$  and  $1/R_2$  are the principal curvatures on the surface, and (4) the integral Gaussian curvature

$$V_3 = \frac{1}{4\pi V} \int_{\partial M} \frac{1}{R_1 R_2} d^2A. \quad (4)$$

The last quantity is proportional to the Euler characteristic of the contour surfaces. The Euler characteristic is also proportional to the genus statistic if the boundary of the sample is neglected. Further geometrical meanings of MFs are found in Mecke, Buchert & Wagner (1994).

### 2.2. Prediction for First- and Second-order Perturbations

#### 2.2.1. Gaussian random field

The analytic formulae of the MFs as functions of the threshold  $\nu$  for random Gaussian field is given by (Tomita 1986; Schmalzing & Buchert 1997):

$$V_k(\nu) = \frac{1}{(2\pi)^{(k+1)/2}} \frac{\omega_3}{\omega_{3-k}\omega_k} \left( \frac{\sigma_1^2}{3\sigma_0^2} \right)^{k/2} H_{k-1}(\nu) e^{-\nu^2/2}, \quad (5)$$

where  $k = 0, 1, 2, 3$ , and the factor  $\omega_k$  is the volume of the unit ball in  $k$ -dimensions, i.e.,  $\omega_0 = 1$ ,  $\omega_1 = 2$ ,  $\omega_2 = \pi$ , and  $\omega_3 = 4\pi/3$ . The quantities  $\sigma_0^2$  and  $\sigma_1^2$  are defined by

$$\sigma_0^2 \equiv \langle \delta^2 \rangle, \quad \sigma_1^2 \equiv \langle (\nabla \delta)^2 \rangle, \quad (6)$$

and the functions  $H_n (n = 0, 2, 3, \dots)$  are the Hermite polynomials with a convention,

$$H_n(\nu) = e^{\nu^2/2} \left( -\frac{\partial}{\partial \nu} \right)^n e^{-\nu^2/2}. \quad (7)$$

Following Matsubara (2003), we use a notation

$$H_{-1}(\nu) \equiv e^{\nu^2/2} \int_{\nu}^{\infty} d\nu' e^{-\nu'^2/2} = \sqrt{\frac{\pi}{2}} e^{\nu^2/2} \operatorname{erfc} \left( \frac{\nu}{\sqrt{2}} \right), \quad (8)$$

when  $k = 0$ .

### 2.2.2. Non-Gaussian field

In non-Gaussian random fields, analytic formula with effects of the weakly non-linear evolution are also derived (Matsubara 2003). Using the Edgeworth-like expansion, the formulae is given by

$$V_k(\nu) = \frac{1}{(2\pi)^{(k+1)/2}} \frac{\omega_3}{\omega_{3-k}\omega_k} \left( \frac{\sigma_1}{\sqrt{3}\sigma_0} \right)^k e^{-\nu^2/2} \left\{ H_{k-1}(\nu) + \left[ \frac{1}{6} S^{(0)} H_{k+2}(\nu) + \frac{k}{3} S^{(1)} H_k(\nu) + \frac{k(k-1)}{6} S^{(2)} H_{k-2}(\nu) \right] \sigma_0 + \mathcal{O}(\sigma_0^2) \right\}, \quad (9)$$

where  $S^{(a)}$  ( $a = 0, 1, 2$ ) are the skewness parameters which are defined by

$$S^{(0)} \equiv \frac{\langle \delta^3 \rangle}{\sigma_0^3}, \quad (10)$$

$$S^{(1)} \equiv -\frac{3}{4} \frac{\langle \delta^2 (\nabla^2 \delta) \rangle}{\sigma_1^2 \sigma_0^2}, \quad (11)$$

$$S^{(2)} \equiv -\frac{9}{4} \frac{\langle (\nabla \delta \cdot \nabla \delta) \nabla^2 \delta \rangle}{\sigma_1^4}. \quad (12)$$

The above formula is a general one for weakly non-Gaussian fields.

In second-order perturbation theory, the skewness parameters of a smoothed density field, convolved with a Gaussian smoothing kernel are given by

$$S^{(0)}(R) = (2 + E)S_0^{11} - 3S_1^{02} + (1 - E)S_2^{11}, \quad (13)$$

$$S^{(1)}(R) = \frac{3}{2} \left[ \frac{5 + 2E}{3} S_0^{13} - \frac{9 + E}{5} S_1^{22} - S_1^{04} + \frac{2(2 - E)}{3} S_2^{13} - \frac{1 - E}{5} S_3^{22} \right], \quad (14)$$

$$S^{(2)}(R) = 9 \left[ \frac{3 + 2E}{15} S_0^{33} - \frac{1}{5} S_1^{24} - \frac{3 + 4E}{21} S_2^{33} + \frac{1}{5} S_3^{24} - \frac{2(1 - E)}{35} S_4^{33} \right], \quad (15)$$

where the factor  $S_m^{\alpha\beta}(R)$  is defined by

$$S_m^{\alpha\beta}(R) \equiv \frac{\sqrt{2\pi}}{\sigma_0^4} \left( \frac{\sigma_0}{\sigma_1 R} \right)^{\alpha+\beta-2} \int \frac{l_1^2 dl_1}{2\pi^2 R^3} \frac{l_2^2 dl_2}{2\pi^2 R^3} P_{\text{lin}} \left( \frac{l_1}{R} \right) P_{\text{lin}} \left( \frac{l_2}{R} \right) e^{-l_1^2 - l_2^2} l_1^{\alpha-3/2} l_2^{\beta-3/2} I_{m+1/2}(l_1 l_2), \quad (16)$$

and  $R$  is a smoothing length,  $I_\nu(z)$  is the modified Bessel function. In linear theory, the variances  $\sigma_0^2$  and  $\sigma_1^2$  are given by

$$\sigma_j^2(R) = \int \frac{k^2 dk}{2\pi^2} k^{2j} P_{\text{lin}}(k) W^2(kR), \quad (17)$$

with  $j = 0, 1$ . In this paper we only consider the Gaussian smoothing kernel  $W_R(x) = \pi^{-3/2} R^{-3} \exp(-x^2/2R^2)$  and thus the window function is given by  $W(kR) = e^{-(kR)^2}$  which is a Fourier transform of the smoothing kernel. The notation  $P_{\text{lin}}(k)$  indicates the linear power spectrum. The constant  $E$  depends on the cosmological parameters and is approximately equal to  $3/7$  (Matsubara 2003) for many sensible models. The values of the skewness parameters are independent on the amplitude of the linear power spectrum in a lowest-order approximation. The linear power spectrum is given by the adiabatic CDM model with Harrison-Zel'dovich spectrum (Bardeen et al. 1986). Neglecting other components, such as baryons and neutrinos, the skewness parameters  $S^{(a)}$  ( $a = 0, 1, 2$ ) are functions of only a combination  $\Gamma R$  where  $\Gamma$  is the shape parameter of the CDM transfer function. The shape parameter  $\Gamma = 0.2$  is adopted in our  $N$ -body simulation of this paper. In Table 1, the values of  $\sigma_0$ ,  $\sigma_1$  in linear theory, and the skewness parameters in second-order perturbation theory are shown for various smoothing lengths, assuming the same cosmological parameters as that of the simulation.

In Figure 1, we plot the functions of equation (9). The skewness parameters in this Figure are calculated by assuming  $\Gamma R = 4.0$ . The curves of  $\sigma_0 = 0.1, 0.2, 0.3, 0.4$  are depicted. The curves with the label  $\sigma_0 = 0.0$  correspond to the Gaussian limit  $\sigma_0 \rightarrow 0$ .

TABLE 1  
THE ANALYTICAL VALUES OF  $\sigma_0$ ,  $R\sigma_1/\sigma_0$  AND THE SKEWNESS PARAMETERS  $S^{(a)}$  CALCULATED IN THE CDM MODEL. THE SHAPE PARAMETER  $\Gamma = 0.2$  AND AN APPROXIMATION  $E = 3/7$  ARE ADOPTED. THE POWER SPECTRUM IS NORMALIZED BY  $\sigma_8 = 0.9$ .

| $R(h^{-1}\text{Mpc})$ | 10    | 12    | 15    | 18    | 20    | 25    | 30    | 40    | 50    |
|-----------------------|-------|-------|-------|-------|-------|-------|-------|-------|-------|
| $\Gamma R$            | 2.0   | 2.4   | 3.0   | 3.6   | 4.0   | 5.0   | 6.0   | 8.0   | 10.0  |
| $\sigma_0$            | 0.394 | 0.328 | 0.258 | 0.210 | 0.185 | 0.141 | 0.111 | 0.075 | 0.054 |
| $R\sigma_1/\sigma_0$  | 0.990 | 1.018 | 1.052 | 1.079 | 1.095 | 1.127 | 1.153 | 1.191 | 1.220 |
| $S^{(0)}$             | 3.500 | 3.453 | 3.398 | 3.355 | 3.332 | 3.285 | 3.250 | 3.201 | 3.169 |
| $S^{(1)}$             | 3.566 | 3.514 | 3.453 | 3.404 | 3.377 | 3.324 | 3.284 | 3.228 | 3.191 |
| $S^{(2)}$             | 3.662 | 3.668 | 3.679 | 3.692 | 3.701 | 3.723 | 3.744 | 3.783 | 3.818 |

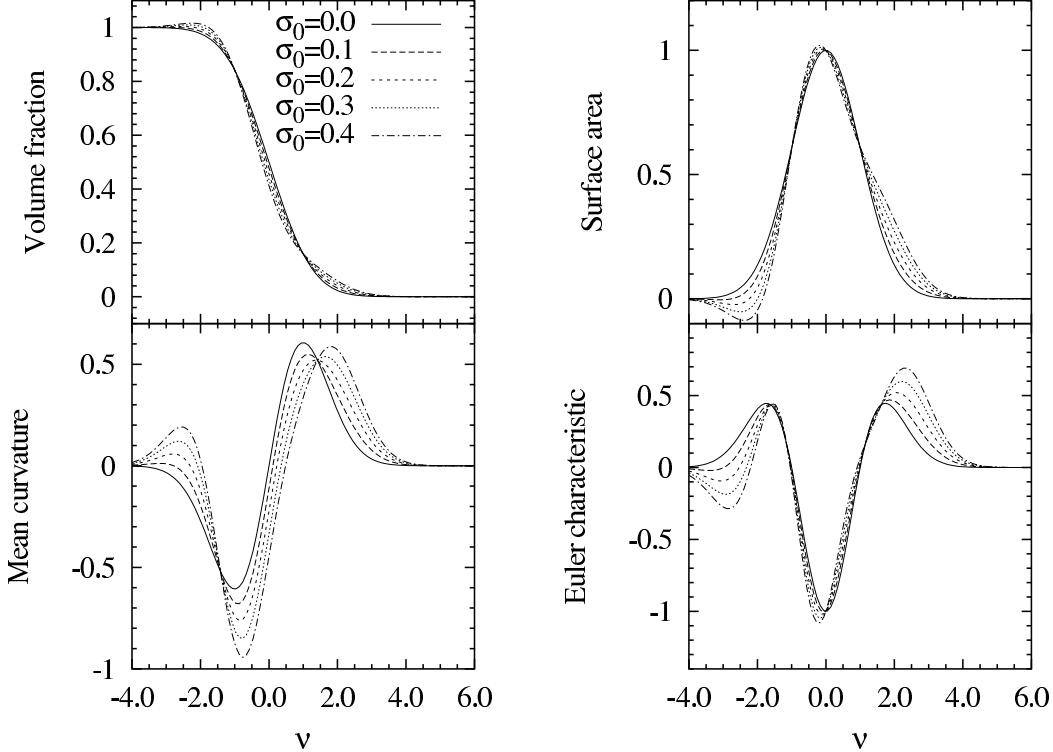


FIG. 1.— The MFs for Gaussian and weakly non-Gaussian random fields. The solid lines with label  $\sigma_0 = 0$  correspond to a Gaussian field. Other curves with  $\sigma_0 = 0.1, 0.2, 0.3, 0.4$  correspond to the weakly non-Gaussian field.

### 2.3. Conversion of the Threshold Density by Volume Fractions

Although we have used the threshold density  $\nu = \delta_{\text{th}}/\sigma_0$  so far, we can use another definition of the threshold  $\nu_f$  (GMD) by the volume fraction of the high-density regions:

$$V_0 = \frac{1}{\sqrt{2\pi}} \int_{\nu_f}^{\infty} dx e^{-x^2/2}. \quad (18)$$

In random Gaussian fields, the two definitions of  $\nu$  and  $\nu_f$  are identical. In most of the previous work on the genus analysis, the rescaled threshold  $\nu_f$  is commonly employed. This re-scaling removes exactly the effect of the evolution of the one-point probability distribution of the density field. Since the two-point characteristics of the density field only affect the MF curves through the parameters  $\sigma_0$  and  $\sigma_1$ , the remaining differences must be due to higher-order characteristics.

Analytic formulae of the MFs by the threshold  $\nu_f$  is given by (Matsubara 2003)

$$V_k(\nu_f) = \frac{1}{(2\pi)^{(k+1)/2}} \frac{\omega_3}{\omega_{3-k}\omega_k} \left( \frac{\sigma_1}{\sqrt{3}\sigma_0} \right)^k e^{-\nu_f^2/2} \left\{ H_{k-1}(\nu_f) + \left[ \frac{k}{3}(S^{(1)} - S^{(0)})H_k(\nu_f) + \frac{k(k-1)}{6}(S^{(2)} - S^{(0)})H_{k-2}(\nu_f) \right] \sigma_0 + \mathcal{O}(\sigma_0^2) \right\}. \quad (19)$$

The highest-order Hermite polynomial in the weakly non-Gaussian terms vanishes in each case. Moreover, the skewness parameters only appear in the form of differences,  $S^{(a)} - S^{(0)}$  ( $a = 1, 2$ ). Therefore, the resultant equation with  $\nu_f$  is simpler than the original form using the threshold  $\nu$ . Because the values of skewness parameters are usually close, the non-Gaussian correction is small with the rescaled threshold  $\nu_f$ .

TABLE 2  
MODEL PARAMETERS OF OUR  $N$ -BODY SIMULATION.

| Model         | No. of particles | Physical box size      | $\Omega_0$ | $\lambda_0$ | $h$    | $\sigma_8$ | $\Gamma$ |
|---------------|------------------|------------------------|------------|-------------|--------|------------|----------|
| $\Lambda$ CDM | $512^3$          | $1024h^{-1}\text{Mpc}$ | 0.30       | 0.70        | 0.6667 | 0.90       | 0.2      |

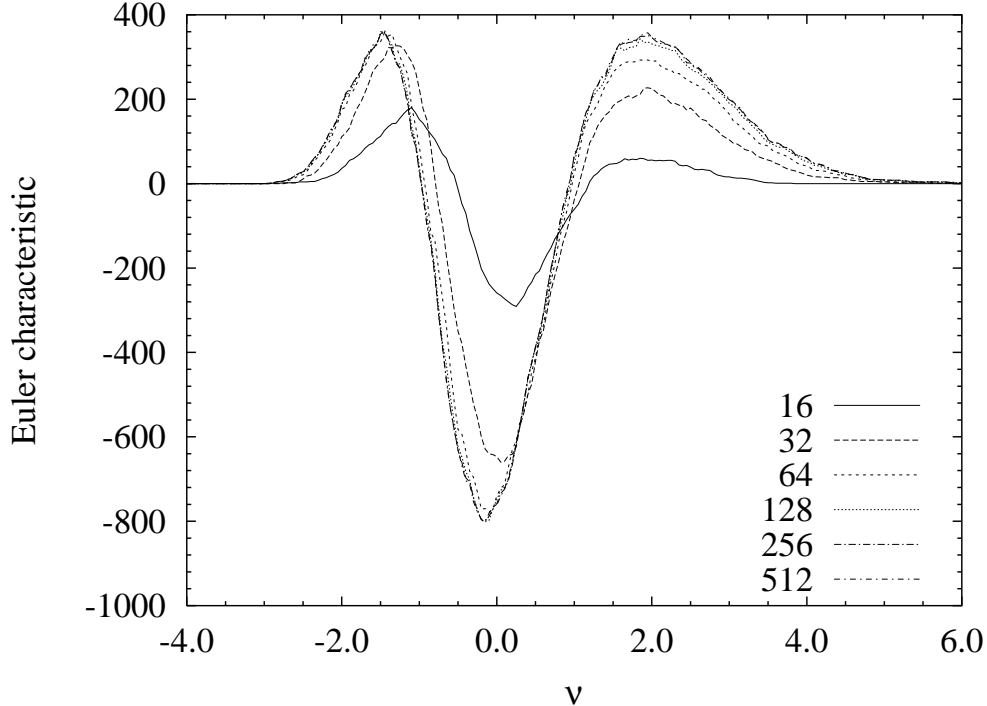


FIG. 2.— The dependence of Euler characteristic on the number of grid points. The smoothing length is fixed to  $20h^{-1}\text{Mpc}$ . One-dimensional grid numbers are 16, 32, 64, 128, 256 and 512 as indicated in the figure. The curve does not converge and behave awkwardly when we adopt the grid number of 16 or 32. On the other hand, the curves of 128, 256, 512 are difficult to distinguish in the figure, thus the result is converged.

Our  $N$ -body simulation is similar to the one carried out by Jing, & Suto (2002), but the physical box size  $1024h^{-1}\text{Mpc}$  is much larger than that. The number of particles is the same,  $N = 512^2$ . This simulation was carried out with the particle-particle-particle-mesh (P<sup>3</sup>M) code on the vector-parallel machine VPP5000 at the National Astronomical Observatory of Japan.

The assumed cosmological model is a flat CDM model with a cosmological constant ( $\Omega_0 = 0.3$ ,  $\lambda_0 = 0.7$ ). The primordial density fluctuations are assumed to be random Gaussian, and the power spectrum is given by the Harrison-Zel'dovich spectrum. The linear transfer function for the power spectrum of the dark matter is that for adiabatic CDM fluctuations. We use the fitting formula by Bardeen et al. (1986) with the shape parameter  $\Gamma = \Omega_0 h = 0.2$ . The amplitude of the power spectrum is determined by  $\sigma_8 = 0.9$  at the present time. Table 2 shows the parameters in this simulation.

In studying MFs, we first generate a continuous density field of galaxies. In order to handle the continuous field, we set the grids in the simulation box. Then the field smoothing is applied in Fourier space, since the direct convolution in real space is much slower to compute. The larger the grid number is, the more precisely the density field is approximated. However, the large number of points requires a long time to compute. We need to find an appropriate number of grid points, keeping the calculation as accurate as possible.

In Figure 2, the Euler characteristic calculated from the  $N$ -body simulation are plotted. The smoothing length is fixed to  $20h^{-1}\text{Mpc}$ , and the number of grid is varied from  $16^3$  to  $512^3$ . The values of the Euler characteristic converge when the grid number is large as expected. Since  $256^3$  and  $512^3$  grids essentially give the same result, we consider results with  $256^3$  grids are accurate enough. The  $128^3$  grids already give reasonable approximation. Similar tendencies are seen in other MFs. We conclude that the grid number is sufficient when the spacing of the grids is larger than  $R/2.5$ . Therefore, as long as  $R \gtrsim 10h^{-1}\text{Mpc}$ ,  $256^3$  grids in our simulation box  $(1024h^{-1}\text{Mpc})^3$  are enough.

Next, we explain error estimation methods in calculating the MFs from the data of the  $N$ -body simulation. The comparison between the analytic formulae in weakly non-linear regions and the MFs calculated from the  $N$ -body simulation can be properly done only if we estimate the correct errors in the simulation. There is a constraint in this work that we have only one set of the  $N$ -body simulation data. If there is only one set of data, we can obtain only one set of the MFs. To calculate the errors, first we divide the cubic box of the  $N$ -body simulation into eight sub-cubes, and then obtain the values of MFs in each cubes. The errors are estimated by their averages and variances divided by a scaling factor,  $\sqrt{7}$ .

TABLE 3  
THE VALUES OF  $\sigma_0$ ,  $R\sigma_1/\sigma_0$  AND THE SKEWNESS PARAMETERS  $S^{(a)}$  FROM NUMERICAL CALCULATIONS OF EQUATIONS (10)-(12) BY THE  $N$ -BODY SIMULATION.

| $R(h^{-1}\text{Mpc})$ | 10                | 12                | 15                | 18                |
|-----------------------|-------------------|-------------------|-------------------|-------------------|
| $\sigma_0$            | $0.378 \pm 0.004$ | $0.314 \pm 0.003$ | $0.258 \pm 0.004$ | $0.201 \pm 0.003$ |
| $R\sigma_1/\sigma_0$  | $0.968 \pm 0.005$ | $0.992 \pm 0.006$ | $1.024 \pm 0.006$ | $1.051 \pm 0.006$ |
| $S^{(0)}$             | $3.505 \pm 0.117$ | $3.425 \pm 0.175$ | $3.398 \pm 0.212$ | $3.368 \pm 0.299$ |
| $S^{(1)}$             | $3.617 \pm 0.095$ | $3.496 \pm 0.121$ | $3.453 \pm 0.138$ | $3.350 \pm 0.183$ |
| $S^{(2)}$             | $3.800 \pm 0.113$ | $3.699 \pm 0.133$ | $3.679 \pm 0.159$ | $3.601 \pm 0.190$ |

| $R(h^{-1}\text{Mpc})$ | 20                | 25                | 30                | 40                | 50                |
|-----------------------|-------------------|-------------------|-------------------|-------------------|-------------------|
| $\sigma_0$            | $0.177 \pm 0.003$ | $0.135 \pm 0.002$ | $0.107 \pm 0.002$ | $0.072 \pm 0.003$ | $0.054 \pm 0.003$ |
| $R\sigma_1/\sigma_0$  | $1.066 \pm 0.008$ | $1.098 \pm 0.014$ | $1.122 \pm 0.023$ | $1.157 \pm 0.042$ | $1.186 \pm 0.061$ |
| $S^{(0)}$             | $3.379 \pm 0.369$ | $3.418 \pm 0.603$ | $3.480 \pm 0.912$ | $3.926 \pm 1.641$ | $5.244 \pm 2.607$ |
| $S^{(1)}$             | $3.347 \pm 0.220$ | $3.370 \pm 0.350$ | $3.376 \pm 0.562$ | $3.346 \pm 1.194$ | $3.673 \pm 1.859$ |
| $S^{(2)}$             | $3.623 \pm 0.211$ | $3.739 \pm 0.309$ | $3.841 \pm 0.504$ | $3.873 \pm 1.392$ | $4.015 \pm 2.569$ |

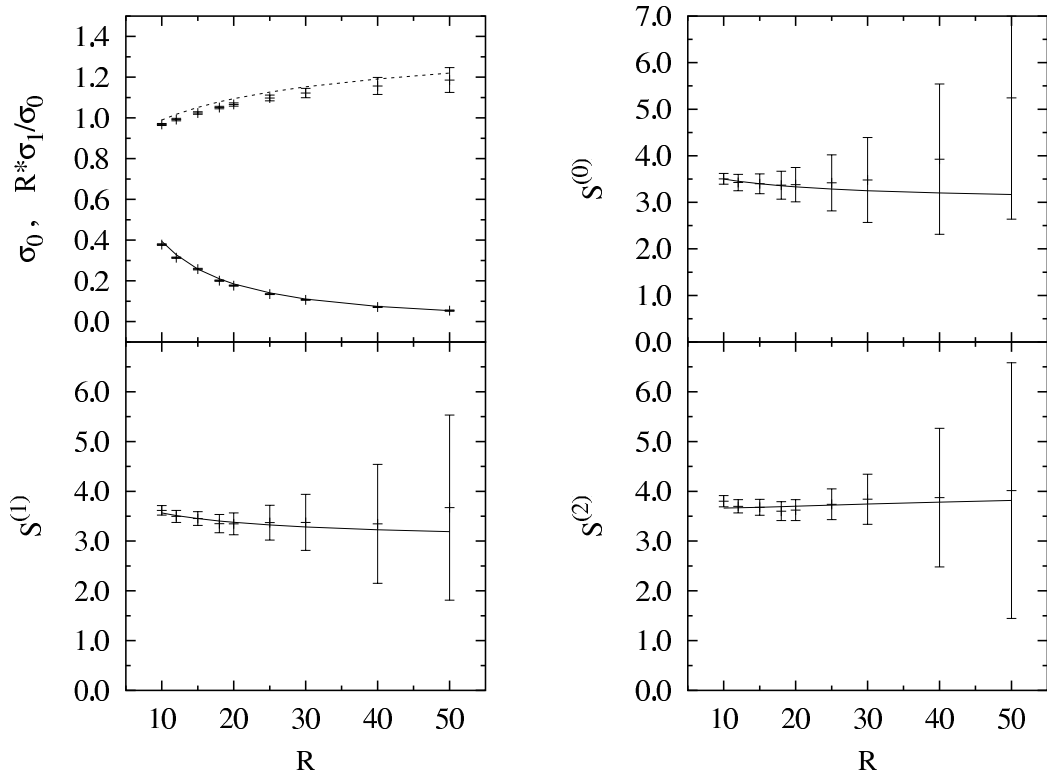


FIG. 3.— The values of  $\sigma_0$ ,  $R \times \sigma_1/\sigma_0$  and the skewness parameters  $S^{(a)}$ . The analytical values are shown with lines, and the values of the  $N$ -body simulation are shown with symbol. 1  $\sigma$  error bars are also shown for the parameters of the  $N$ -body simulation.

## 4. RESULTS

### 4.1. The values of the skewness parameters

Before examining the MFs, we first calculate the skewness parameters from the simulation, since these parameters are essential in analytic formulae of the MFs. Table 3 and Figure 3 show the standard deviation  $\sigma_0$  of the density distribution of the galaxy  $\delta$ ,  $R\sigma_1/\sigma_0$ , and the skewness parameters of equations (10)-(12) calculated numerically from the  $N$ -body simulation. We use  $256^3$  grids commonly for each smoothing length. In Figure 3, the analytic predictions and numerical values from the simulation of these parameters are compared.

As obviously seen in Figure 3, most of the figures agree within the range of numerical errors. There have been similar studies comparing analytic and numerical values of  $S^{(a)}$  and disagreements are reported (e.g., Colley et al. 2000; Hikage, Taruya, & Suto 2003b). One of the reason of the disagreements is that those samples are not large enough in volume and hence the calculations of the skewness parameters are affected by the cosmic variance. Other reason is that the previous work uses biased sample in the simulation. Our comparison is directly made by the dark matter distribution in order to separate the complex biasing effects and

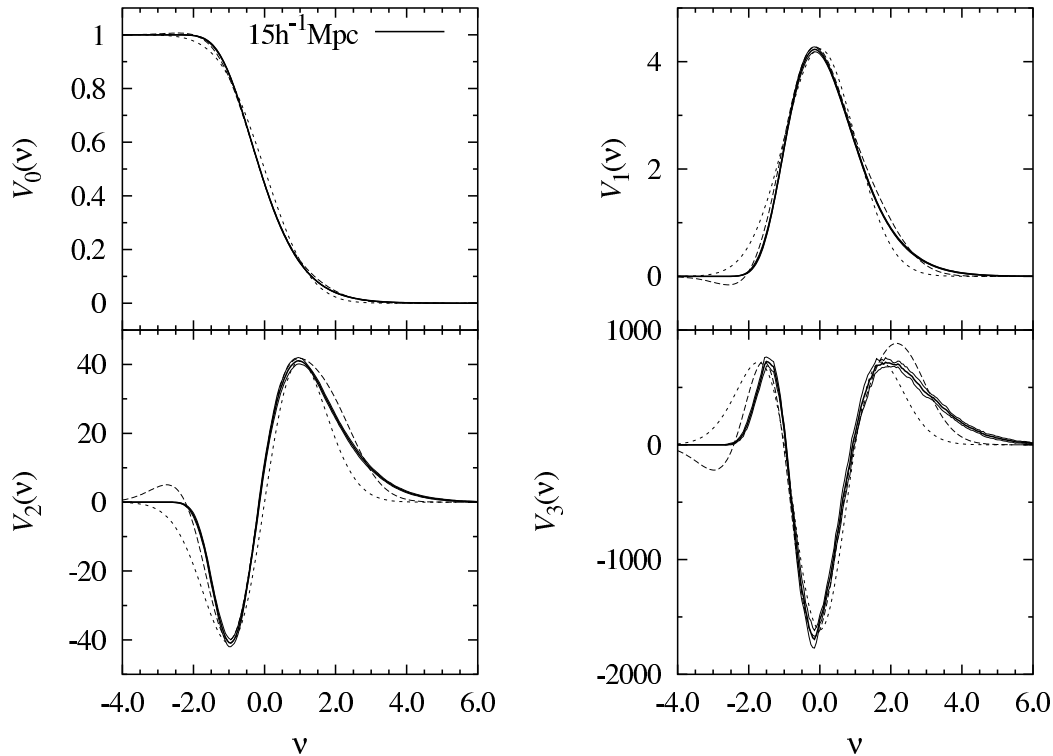


FIG. 4.— The comparison of the MFs for the threshold  $\nu$  at the smoothing length  $R = 15h^{-1}\text{Mpc}$ . *Thick solid lines*: the MFs calculated from  $N$ -body simulation; *thin solid lines*:  $1\sigma$  errors; *short-dashed lines*: analytical curves for Gaussian random field; *long-dashed lines*: analytical curves for weakly non-linear evolution.

to concentrate on purely nonlinear evolution.

There are some disagreements in the values of  $\sigma_0$  and  $\sigma_1$ , which are expected if we take into account the fact that non-linear corrections of order  $\sigma_0^2$  should be added to the linear predictions of  $\sigma_0$ . Without the second-order correction, the theoretical values of  $\sigma_0$  have a tendency to the underestimation. This can be understood by the fact that the correlation function integrated over whole space have to be zero while the powers on small scales are enhanced by nonlinear evolution. Consequently, the powers on weakly nonlinear scales are suppressed and the linear predictions of  $\sigma_0$  overestimates the power (Peacock, & Dodds 1994, 1996).

#### 4.2. The comparison of the Minkowski Functionals between the $N$ -body simulation and the analytic formulae

In this section, we compare the MFs calculated from the  $N$ -body simulation with the analytic formulae. The calculation method of the MFs of the  $N$ -body simulation is based on Crofton's formula (Crofton 1868), derived from integral geometry (for details, see Schmalzing & Buchert 1997). Figures 4, 5 and 6 show the four MFs  $V_k(\nu)$  ( $k = 0, 1, 2, 3$ ). Each MF is calculated adopting smoothing lengths of 15, 25, and  $50h^{-1}\text{Mpc}$ . The analytic formulae of the Gaussian random fields are plotted with short-dashed lines, and those of the weakly non-linear fields with long-dashed lines. The amplitudes of the analytic curves are estimated by calculating  $\sigma_0$  and  $\sigma_1$  directly from the  $N$ -body simulation.

Figure 7 shows the differences between the MFs of the  $N$ -body simulation and that of the analytic formulae. In the plots, the differences divided by the  $1\sigma$  errors of  $N$ -body data are shown. Thus if the curves are in the range of  $(-1, +1)$ , the two curves are consistent with  $1\sigma$  significance. As expected, the MFs calculated from the  $N$ -body simulation agree with the analytic formulae for large smoothing lengths.

For quantitative comparisons, we calculate the mean differences between normalized MF values of the analytic prediction and that of the simulation:

$$D_k \equiv \frac{1}{|V_k(\text{max})|} \sqrt{\frac{1}{N} \sum_{i=1}^N [V_k^{(A)}(\nu_i) - V_k^{(S)}(\nu_i)]^2}, \quad (20)$$

where superscript (A) stands for ‘‘analytic’’ and (S) stands for ‘‘simulation’’, and  $V_k(\text{max})$  is the maximum value of a MF  $V_k$  evaluated by the Gaussian formula, i.e.,  $V_0(\nu = -\infty) = 1$ ,  $V_1(\nu = 0)$ ,  $V_2(\nu = 1)$  and  $V_3(\nu = 0)$  for  $k = 0, 1, 2, 3$ , respectively. The set of various thresholds  $\nu_i$  are given by choosing  $N = 121$  equally spaced points with interval  $\Delta\nu = 0.05$  in the range  $-2 \leq \nu \leq +4$ .

When the mean differences defined above are within errors of the numerical simulation, the indicated differences are not distinguished from real differences between analytic predictions and true values of MFs. Therefore, we also define the mean

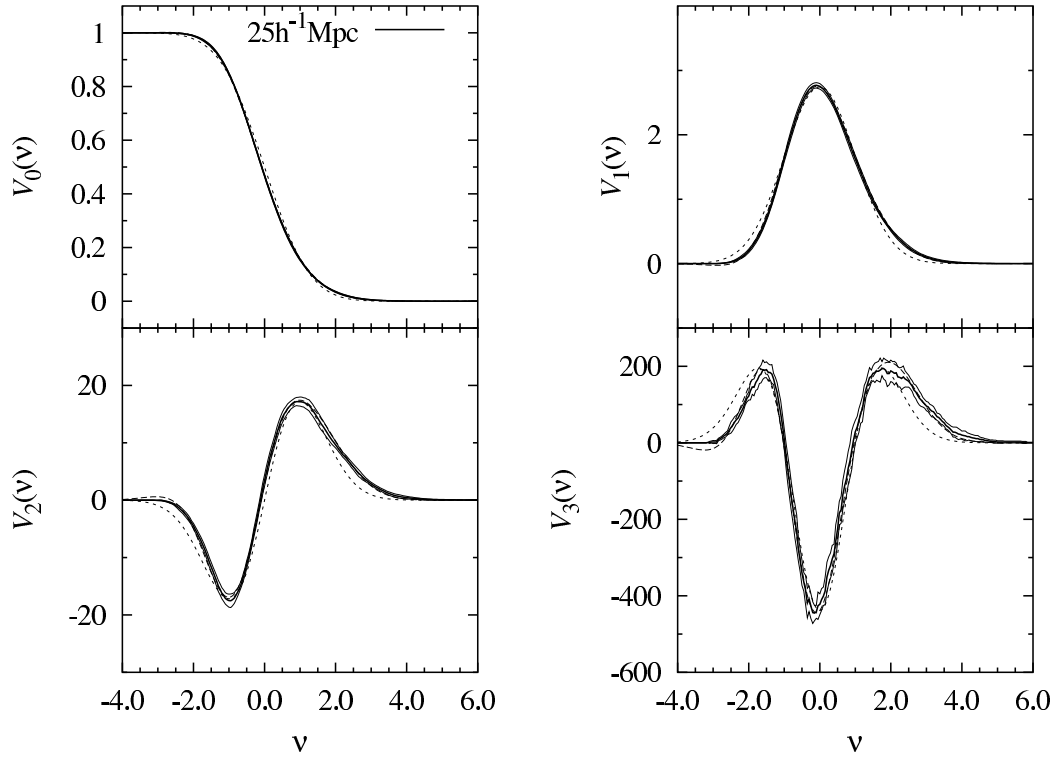


FIG. 5.— Same as figure 4, but for the smoothing length  $R = 25h^{-1}\text{Mpc}$ .

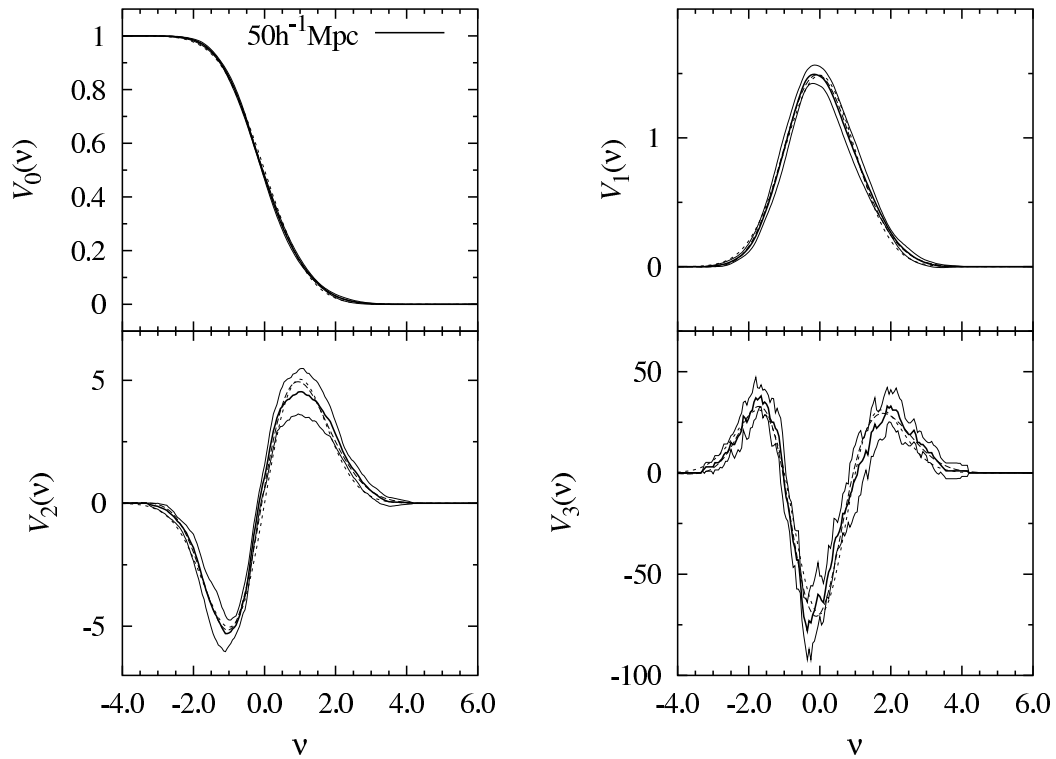


FIG. 6.— Same as figure 4, but for the smoothing length  $R = 50h^{-1}\text{Mpc}$ .



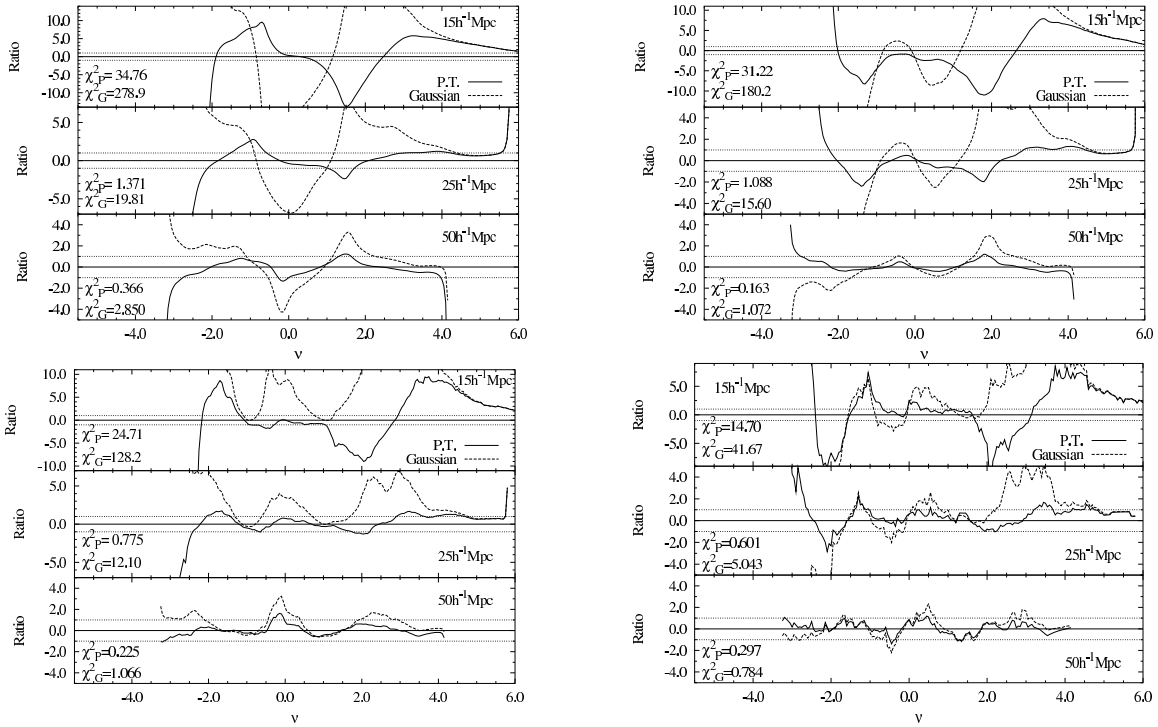


FIG. 7.— The ratio of difference between the MFs of  $N$ -body simulation and the analytical values to the error at the smoothing lengths  $R=15, 25$  and  $50h^{-1}\text{Mpc}$ . *Upper left panel*: the volume fraction; *upper right panel*: the surface area; *lower left panel*: the integrated mean curvature; *lower right panel*: the Euler characteristic.  $\chi^2_{\text{P.T.}}/\text{d.o.f.}$  and  $\chi^2_{\text{Gaussian}}/\text{d.o.f.}$  calculated in the range  $-2 \leq \nu \leq +4$  are also shown.

errors of the normalized MFs in simulation data,

$$E_k \equiv \frac{1}{V_k(\text{max})} \sqrt{\frac{1}{N} \sum_{i=1}^N [\Delta V_k^{(S)}(\nu_i)]^2}, \quad (21)$$

and the chi-square per degree of freedom:

$$\hat{\chi}^2 = \frac{1}{N} \sum_{i=1}^N \frac{[V_k^{(A)}(\nu_i) - V_k^{(S)}(\nu_i)]^2}{[\Delta V_k^{(S)}(\nu_i)]^2}, \quad (22)$$

where  $\Delta V_k^{(S)}(\nu_i)$  indicate the  $1\sigma$  errors in the simulation data. When  $D_k \lesssim E_k$ , the indicated differences are within the errors originated from a numerical resolution of the simulation, and are not considered as real differences. In fact, this criterion is consistent with a usual chi-square criterion  $\hat{\chi}^2 \lesssim 1$ . When  $\hat{\chi}^2 \gtrsim 1$ , the differences are interpreted as deviations of the analytic predictions from true values of MFs. Thus accuracies of the analytic predictions are indicated by the quantity  $D_k$  when  $\hat{\chi}^2 \gtrsim 1$ . On the other hand, when  $\hat{\chi}^2 \lesssim 1$ , the statistic  $D_k$  represent the upper limits of the accuracies.

In Table 4, the above statistics are shown for all MFs. In the Table,  $D_k^{(2\text{nd})}$  and  $D_k^{(\text{lin})}$  indicate the equation (20) for 2nd-order and linear perturbation theory, respectively. Likewise,  $\hat{\chi}_{2\text{nd}}^2$  and  $\hat{\chi}_{\text{lin}}^2$  indicate the equation (22) for 2nd-order and linear perturbation theory, respectively.

Overall, since  $D_k^{(2\text{nd})}$  are smaller than  $D_k^{(\text{lin})}$  in each case, the second-order predictions show better agreement with simulation data. For example, a prediction of the second-order theory of  $V_3$  agrees with the simulation data by 4% accuracy level, while that of the linear theory agrees by 10% level. In other words, the chi-square statistics of the second-order theory are always smaller than that of the linear theory. Since the linear theory is less accurate approximation than the second-order theory, this is a natural consequence. When the smoothing lengths are large, the differences between second-order predictions and the simulation data are not distinguishable. There are two reasons for this tendency. First, the analytic predictions are more accurate on large scales. Second, the simulation data suffers more errors by finite volume effects.

On smaller scales,  $R \sim 10h^{-1}\text{Mpc}$ , the analytic predictions of the perturbation theories are less accurate because of the nonlinear evolutions. Even in this regime, the second-order theory is more accurate than the linear theory. Therefore, the predictions of the second-order theory is always better than that of the linear theory in the regime we investigate, i.e.,  $10h^{-1}\text{Mpc} \lesssim R \lesssim 50h^{-1}\text{Mpc}$ .

At this point, one should note that there are correlations between the adjacent thresholds  $\nu_i$  and  $\nu_{i+1}$ . If the value of the MFs increases (decreases) at some threshold density  $\nu_i$ , there is higher possibility that the value also increases (decreases) at the next

TABLE 4  
VALUES OF  $D_k$  OF EQUATION (20),  $E_k$  OF EQUATION (21), AND  $\widehat{\chi}^2$  OF EQUATION (22).

| $k$ | Smoothing Length $R(h^{-1}\text{Mpc})$ |        |        |        |        |        |        |
|-----|--|--------|--------|--------|--------|--------|--------|
|     | 10                                     | 15     | 20     | 25     | 40     | 50     |        |
| 0   | $D_k^{(2\text{nd})}$                   | 0.27%  | 0.050% | 0.016% | 0.010% | 0.013% | 0.017% |
|     | $D_k^{(\text{linear})}$                | 1.58%  | 0.70%  | 0.38%  | 0.24%  | 0.14%  | 0.15%  |
|     | $E_k$                                  | 0.003% | 0.003% | 0.005% | 0.010% | 0.030% | 0.056% |
|     | $\widehat{\chi}_{2\text{nd}}^2$        | 3631   | 34.76  | 5.950  | 1.371  | 0.314  | 0.366  |
|     | $\widehat{\chi}_{\text{fin}}^2$        | 13317  | 278.9  | 66.29  | 19.81  | 3.608  | 2.850  |
|     | $D_k^{(2\text{nd})}$                   | 7.6%   | 3.0%   | 1.8%   | 1.6%   | 2.0%   | 1.8%   |
| 1   | $D_k^{(\text{linear})}$                | 12%    | 6.9%   | 5.2%   | 5.2%   | 5.1%   | 4.4%   |
|     | $E_k$                                  | 0.75%  | 0.73%  | 0.99%  | 1.9%   | 5.5%   | 6.3%   |
|     | $\widehat{\chi}_{2\text{nd}}^2$        | 723.9  | 31.22  | 5.284  | 1.088  | 0.136  | 0.163  |
|     | $\widehat{\chi}_{\text{fin}}^2$        | 6678   | 180.2  | 60.63  | 15.60  | 1.610  | 1.072  |
|     | $D_k^{(2\text{nd})}$                   | 14%    | 6.7%   | 4.0%   | 3.1%   | 3.8%   | 6.1%   |
|     | $D_k^{(\text{linear})}$                | 25%    | 18%    | 13%    | 11%    | 9.1%   | 9.6%   |
| 2   | $E_k$                                  | 1.6%   | 2.1%   | 3.0%   | 4.3%   | 9.2%   | 15%    |
|     | $\widehat{\chi}_{2\text{nd}}^2$        | 148.1  | 24.71  | 3.547  | 0.775  | 0.204  | 0.225  |
|     | $\widehat{\chi}_{\text{fin}}^2$        | 3146   | 128.2  | 49.34  | 12.10  | 1.848  | 1.066  |
|     | $D_k^{(2\text{nd})}$                   | 14%    | 7.1%   | 4.5%   | 3.9%   | 5.4%   | 7.7%   |
|     | $D_k^{(\text{linear})}$                | 18%    | 13%    | 10%    | 8.9%   | 9.3%   | 11%    |
|     | $E_k$                                  | 2.3%   | 3.4%   | 4.8%   | 6.1%   | 1.0%   | 14%    |
| 3   | $\widehat{\chi}_{2\text{nd}}^2$        | 265.2  | 14.70  | 2.164  | 0.601  | 0.384  | 0.297  |
|     | $\widehat{\chi}_{\text{fin}}^2$        | 841.0  | 41.67  | 13.06  | 5.043  | 1.513  | 0.784  |

TABLE 5  
SAME AS TABLE 4, BUT FOR THE RESCALED THRESHOLD  $\nu_f$ .

| $k$ | Smoothing length $R(h^{-1}\text{Mpc})$ |       |       |       |       |       |       |
|-----|--|-------|-------|-------|-------|-------|-------|
|     | 10                                     | 15    | 20    | 25    | 40    | 50    |       |
| 1   | $D_k^{(2\text{nd})}$                   | 1.4%  | 0.45% | 0.35% | 0.64% | 1.5%  | 1.3%  |
|     | $D_k^{(\text{linear})}$                | 1.2%  | 0.42% | 0.39% | 0.69% | 2.1%  | 2.4%  |
|     | $E_k$                                  | 0.75% | 0.73% | 0.99% | 1.9%  | 5.5%  | 6.3%  |
|     | $\widehat{\chi}_{2\text{nd}}^2$        | 4.441 | 0.457 | 0.121 | 0.115 | 0.083 | 0.070 |
|     | $\widehat{\chi}_{\text{fin}}^2$        | 1.917 | 0.377 | 0.140 | 0.126 | 0.113 | 0.091 |
|     | $D_k^{(2\text{nd})}$                   | 3.4%  | 1.4%  | 1.4%  | 1.9%  | 3.4%  | 5.5%  |
| 2   | $D_k^{(\text{linear})}$                | 1.5%  | 1.2%  | 1.8%  | 2.5%  | 4.3%  | 6.1%  |
|     | $E_k$                                  | 1.6%  | 2.1%  | 3.0%  | 4.3%  | 9.2%  | 1.5%  |
|     | $\widehat{\chi}_{2\text{nd}}^2$        | 7.397 | 0.687 | 0.248 | 0.206 | 0.221 | 0.196 |
|     | $\widehat{\chi}_{\text{fin}}^2$        | 0.961 | 0.311 | 0.303 | 0.298 | 0.293 | 0.285 |
|     | $D_k^{(2\text{nd})}$                   | 3.2%  | 2.1%  | 2.3%  | 2.6%  | 5.3%  | 7.5%  |
|     | $D_k^{(\text{linear})}$                | 1.4%  | 2.2%  | 3.1%  | 3.5%  | 6.5%  | 8.8%  |
| 3   | $E_k$                                  | 2.4%  | 3.6%  | 5.0%  | 6.2%  | 11%   | 15%   |
|     | $\widehat{\chi}_{2\text{nd}}^2$        | 6.115 | 0.758 | 0.280 | 0.228 | 0.519 | 0.340 |
|     | $\widehat{\chi}_{\text{fin}}^2$        | 0.351 | 0.464 | 0.408 | 0.330 | 0.599 | 0.431 |

threshold density  $\nu_{i+1}$  because of the correlation. This is particularly prominent in the Euler characteristic  $V_3$ . Since the chi-square analysis cannot take such correlations into account, the discrepancies between the theory and the data might be over emphasized.

#### 4.3. The comparison of the MFs in terms of the rescaled thresholds

In the above comparisons, we use the threshold  $\nu = \delta/\sigma_0$ . In the following, we use the rescaled threshold  $\nu_f$  and make the same comparisons. Figures 8, 9 and 10 correspond to Figures 4, 5 and 6, respectively. The differences of the MFs between the analytic formulae and the simulation are also shown in Figure 11.

From these Figures, we find that the differences in terms of  $\nu_f$  are smaller than those in terms of  $\nu$  for all MFs. Mathematically, one of the reason for this is that the skewness parameters only appear as combinations of the form  $S^{(a)} - S^{(0)}$  in the analytic formulae (eq. [19]), and the three values of skewness parameters in CDM cosmological model are close. Since  $S^{(1)} - S^{(0)}$  is almost zero in broad range of the smoothing length, the deviations from analytic formulae are mainly depend on the value of  $S^{(2)} - S^{(0)}$ .

The differences  $D_k$ , errors  $E_k$ , and chi-square per d.o.f.  $\widehat{\chi}^2$  are also calculated in terms of  $\nu_f$ . These statistics are shown in Table 5. It is seen that the differences  $D_k$  are within several percent in almost all MFs. Most of the  $\widehat{\chi}^2$  are less than 1 and the

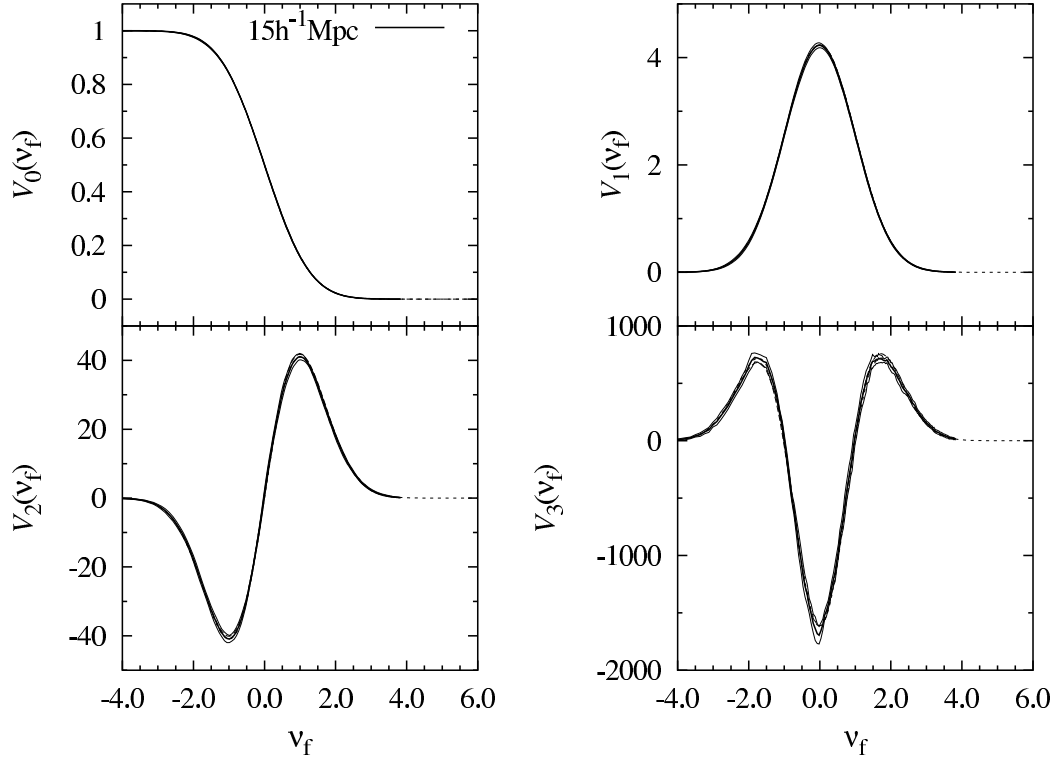


FIG. 8.— Same as Figure 4, but for the threshold density  $\nu_f$  rescaled by volume fraction.

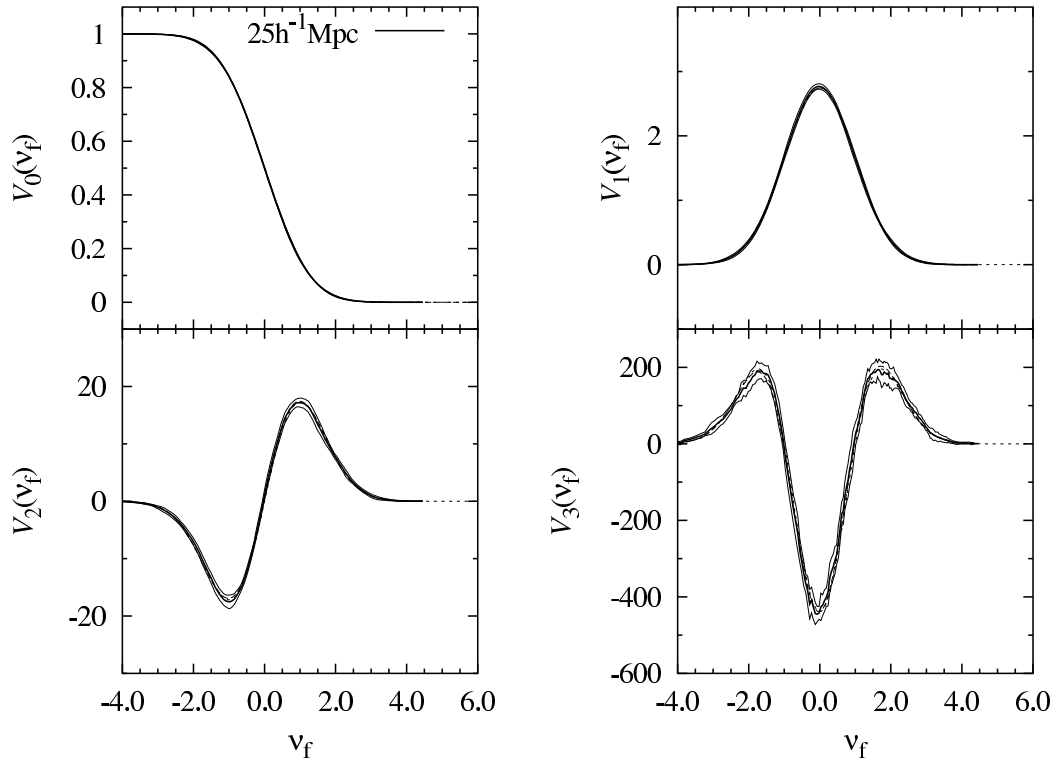


FIG. 9.— Same as Figure 4, but for the smoothing length  $R = 25h^{-1}\text{Mpc}$  and the threshold density  $\nu_f$  rescaled by volume fraction.

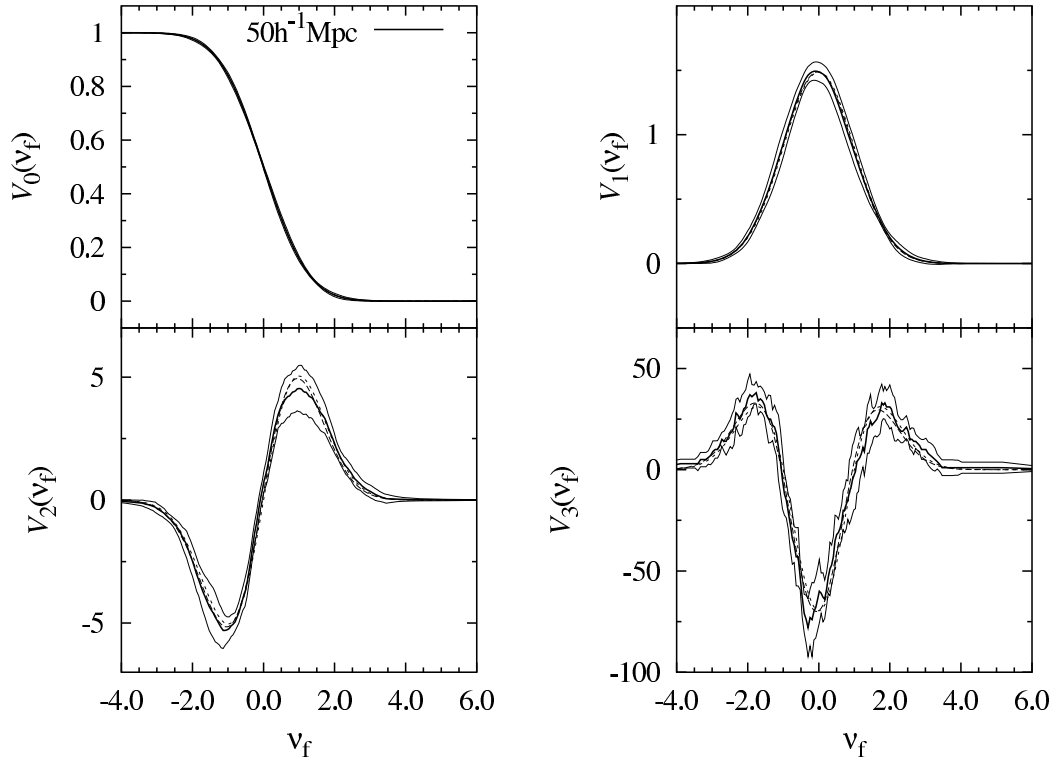


FIG. 10.— Same as Figure 4, but for the smoothing length  $R = 50h^{-1}\text{Mpc}$  the threshold density  $\nu_f$  rescaled by volume fraction.

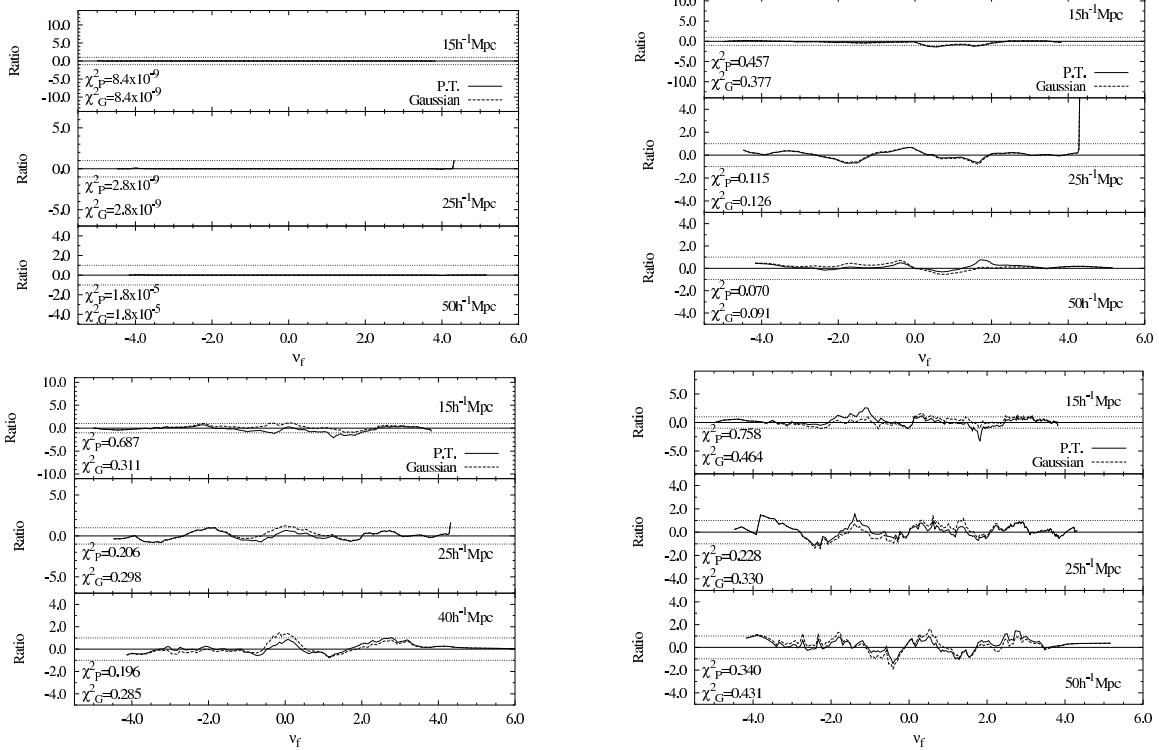


FIG. 11.— Same as Figure 7, but for the threshold density  $\nu_f$  rescaled by volume fraction.

prediction of the analytic formulae are not distinguishable with the simulation results. Interestingly, the second-order predictions of  $V_1$ ,  $V_2$  and  $V_3$  for  $R = 10h^{-1}\text{Mpc}$  are less accurate than the linear predictions. On this scale, both the linear theory and the second-order theory can be inaccurate. A possible interpretation is that the strongly nonlinear dynamics affect the MFs to cancel the second-order correction term in the analytic formulae.

As a result, the linear theory and the second-order theory are difficult to be distinguished when rescaled threshold  $\nu_f$  is used. This is a good news for testing the primordial non-Gaussianity in the density fluctuations since the nonlinear dynamics in course of the density evolution does not significantly alter the shape of MFs in Gaussian fields.

## 5. CONCLUSIONS AND DISCUSSION

We analyze the Minkowski functionals using a large  $N$ -body simulation of a  $\Lambda\text{CDM}$  model with a box size of  $(1024h^{-1}\text{Mpc})^3$  and canonical cosmological parameters,  $\Omega_0 = 0.3$ ,  $\lambda_0 = 0.7$ ,  $h = 0.6667$ ,  $\Gamma = 0.2$ . The detailed analysis of the MFs with such a large  $N$ -body simulation is unprecedented. The validity levels and regions of the analytic formulae of the MFs are studied in detail. We focus on the transition scales from linear to nonlinear evolution,  $10\text{--}50h^{-1}\text{Mpc}$ , and calculate the typical differences of the MFs between the analytic formulae and the  $N$ -body simulation.

The variance parameters  $\sigma_0$ ,  $\sigma_1$ , and the skewness parameters  $S^{(a)}$  ( $a = 0, 1, 2$ ) are calculated from the simulation and compared with analytic predictions. It is found that  $S^{(a)}$  ( $a = 0, 1, 2$ ) agree with the analytic values within the simulation errors in a large range of smoothing lengths. In the previous work of such comparisons, physical sizes of the simulations are not large enough as in this work. Thus the skewness parameters from the simulation suffer from the cosmic variance and disagree with analytic predictions. It is a new result that the skewness parameters calculated from such a large  $N$ -body simulation as  $(1024h^{-1}\text{Mpc})^3$  agree with the analytic predictions. On the other hand, the variance  $\sigma_0$  calculated from the  $N$ -body simulation is slightly smaller than the linear prediction naturally expected in weakly non-linear regime.

In this paper we use two definitions of the threshold density, i.e.,  $\nu$  defined by the value of the density field, and  $\nu_f$  defined by the volume fraction. Nonlinear effects on MFs are stronger against the threshold  $\nu$  than  $\nu_f$ . In most of the previous studies on the topology of the large-scale structure, the threshold density  $\nu_f$  has been adopted. The reason for this choice is that shape of the genus curve is empirically known not to be much affected by the nonlinear evolution. This was also analytically shown in weakly nonlinear regime. In this paper, it is shown that the deviations of the MFs on nonlinear scales are indistinguishable with Gaussian predictions even though we use a large  $N$ -body sample. To detect the effects of the weakly nonlinear evolution in  $\nu_f$  case, a larger sample with less cosmic variance will be needed. Sampling the galaxies in over  $1(h^{-1}\text{Gpc})^3$  comoving volume is within reach of the future surveys. For example, in the SDSS Luminous Red Galaxy survey (Eisenstein et al. 2001), the large-scale structure up to  $z \lesssim 0.5$  is being probed. The covered volume is approximately  $1(h^{-1}\text{Gpc})^3$  in this survey. Therefore, our estimates of the errors of MFs in the simulation roughly correspond to the errors in this kind of surveys. If we have still larger surveys, e.g., a  $z \lesssim 1$  survey with a large sky coverage, the MFs can be measured in exquisite detail. When some non-Gaussian behavior in MFs is observationally found, it is important to distinguish the non-Gaussianity of the primordial density field from that caused by non-linear evolution. This work gives useful information in this respect.

In this work, we use the density distribution in real space. In redshift surveys, the observed distributions of galaxies are in redshift space. The shape of MFs as functions of the threshold is unaffected by peculiar velocity effect in redshift space in linear theory (Matsubara 1996). Analytic formula of MFs in redshift space with nonlinear effect has not been derived yet. In future work, it will be interesting to investigate weakly nonlinear effect on MFs in redshift space, both analytically and numerically.

TM acknowledges support from the MEXT, Grant-in-Aid for Encouragement of Young Scientists, 15740151, 2003. YPJ is supported in part by NKBRSF(G19990754) and NSFC.

## REFERENCES

- Bardeen, J. R., Bond, J. R., Kaiser, N., & Szalay, A. S. 1986, *ApJ*, 304, 15  
 Canavezes, A., et al. 1998, *MNRAS*, 297, 777  
 Colley, W. N. 1997, *ApJ*, 489, 471  
 Colley, W. N., Gott, J. R. I., Weinberg, D. H., Park, C., & Berlind, A. A. 2000, *ApJ*, 529, 795  
 Crofton, M. W. 1868, *Philos. Trans. R. Soc. London*, A158, 181  
 Einasto, J., & Miller, R. H. 1983, *IAU Symposium 104, Early Evolution of the Universe and Its Present Structure*, ed. Abell, G. O., & Chincarni, G. (Dordrecht: Reidel), p. 405  
 Eisenstein, D. J. et al. 2001, *AJ*, 122, 2267  
 Gott, J. R., III, Melott, A. L., & Dickinson, M. 1986, *ApJ*, 306, 341  
 Hikage, C., et al. 2002, *PASJ*, 54, 707  
 Hikage, C., et al. 2003, *PASJ*, 55, 911  
 Hikage, C., Taruya, A., & Suto, Y. 2003, *PASJ*, 55, 335  
 Hikage, C., Suto, Y., Kayo, I., Taruya, A., Matsubara, T., Vogeley, M. S., Hoyle, F., Gott, J. R., III, & Brinkmann, J. 2002, *Publ. Astron. Soc. Japan*, 54, 707  
 Jing, Y. P., & Suto, Y. 1998, *ApJ*, 494, L5  
 Jing, Y. P., & Suto, Y. 2002, *ApJ*, 574, 538  
 Joveer, M., & Einasto, U. 1978, *IAU Symposium 79, The Large Scale Structure of the Universe*, ed. M. S. Longair & J. Einasto (Dordrecht: Reidel), p. 241  
 Matsubara, T. 1996, *ApJ*, 457, 13  
 Matsubara, T. 1994, *ApJ*, 434, L43  
 Matsubara, T. 2003, *ApJ*, 584, 1  
 Mecke, K. R., Buchert, T., & Wagner, H. 1994, *A&A*, 288, 697  
 Minkowski, H. 1903, *Math. Ann.*, 57, 447  
 Miyoshi, K., & Kihara, T. 1975, *Publ. Astron. Soc. Japan*, 27, 333  
 Peacock, J. A., & Dodds, S. J. 1994, *MNRAS*, 267, 1020  
 Peacock, J. A., & Dodds, S. J. 1996, *MNRAS*, 280, L19  
 Schmalzing, J., & Buchert, T. 1997, *ApJ*, 482, L1  
 Seto, N. 2000, *ApJ*, 537, 21  
 Soneira, R. M., & Peebles, P. J. E. 1978, *Astron. J.*, 83, 845  
 Springel, V., et al. 1998, *MNRAS*, 298, 1169  
 Tomita, H. 1986, *Prog. Theor. Phys.*, 76, 952  
 Vogeley, M. S., Park, C., Geller, M. J., Huchra, J. P., & Gott, J. R., III 1994, *ApJ*, 420, 525